

## An Anthracene-Incorporated [8]Cycloparaphenylene Derivative as Emitter in Photon Upconversion

Paolo Della Sala, Amedeo Capobianco, Tonino Caruso, Carmen Talotta, Margherita De Rosa, Placido NERI, Andrea Peluso, and Carmine Gaeta

*J. Org. Chem.*, **Just Accepted Manuscript** • DOI: 10.1021/acs.joc.7b02590 • Publication Date (Web): 12 Dec 2017

Downloaded from <http://pubs.acs.org> on December 15, 2017

### Just Accepted

“Just Accepted” manuscripts have been peer-reviewed and accepted for publication. They are posted online prior to technical editing, formatting for publication and author proofing. The American Chemical Society provides “Just Accepted” as a free service to the research community to expedite the dissemination of scientific material as soon as possible after acceptance. “Just Accepted” manuscripts appear in full in PDF format accompanied by an HTML abstract. “Just Accepted” manuscripts have been fully peer reviewed, but should not be considered the official version of record. They are accessible to all readers and citable by the Digital Object Identifier (DOI®). “Just Accepted” is an optional service offered to authors. Therefore, the “Just Accepted” Web site may not include all articles that will be published in the journal. After a manuscript is technically edited and formatted, it will be removed from the “Just Accepted” Web site and published as an ASAP article. Note that technical editing may introduce minor changes to the manuscript text and/or graphics which could affect content, and all legal disclaimers and ethical guidelines that apply to the journal pertain. ACS cannot be held responsible for errors or consequences arising from the use of information contained in these “Just Accepted” manuscripts.

# An Anthracene-Incorporated [8]Cycloparaphenylene Derivative as Emitter in Photon Upconversion

Paolo Della Sala, Amedeo Capobianco, Tonino Caruso, Carmen Talotta, Margherita De Rosa,  
Placido Neri, Andrea Peluso\* and Carmine Gaeta\*

*Dipartimento di Chimica e Biologia "A. Zambelli", Università di Salerno, Via Giovanni Paolo II 132,  
I-84084 Fisciano (Salerno), Italy,*

*e-mail: [cgaeta@unisa.it](mailto:cgaeta@unisa.it).*

**RECEIVED DATE (to be automatically inserted after your manuscript is accepted if required  
according to the journal that you are submitting your paper to)**



ABSTRACT. The anthracene-incorporated [8]cycloparaphenylene **2** has been synthesized and its optoelectronic properties studied by UV-vis spectroscopy, cyclic voltammetry, and DFT calculations. NMR and computational studies indicate that the new cycloparaphenylene derivative possesses a  $C_s$  point group symmetry. The new CPP **2** exhibits peculiar optoelectronic properties: i) fluorescence emission is blue shifted with respect to [8]cycloparaphenylene **1** and its quantum yield is higher; ii) in the presence of an octaethylporphyrin Pd complex, as sensitizer, it undergoes a visible light upconversion. This is the first case in which a cycloparaphenylene derivative is involved as emitter in low power light frequency conversion.

## INTRODUCTION

CycloParaPhenylenes<sup>1</sup> (CPPs) are conjugated macrocycles consisting of para-linked benzene units (e.g.: **1**, Figure 1),<sup>1</sup> which have originally raised much interest as potential seeds for growing uniform single-walled carbon nanotubes<sup>2</sup> and as supramolecular hosts for the recognition of fullerene<sup>3</sup> and pyridinium guests.<sup>4</sup> Aside from those potential applications, [*n*]CPPs (*n* stands for the number of phenylene rings of the nanohoop) also proved to possess intriguing size dependent optical and electronic properties,<sup>1e</sup> arising from a delicate interplay between the macrocycle strain energy and the  $\pi$ -electron conjugation: *i*) [*n*]CPPs can host up to four electrons (for *n* = 8) without breaking the hoop;<sup>1g</sup> *ii*) they have high optical absorbance, which increases with the number of phenylene rings;<sup>1</sup> *iii*) although they exhibit a common absorbance maximum independent of *n*, their emission is significantly size dependent, being red-shifted as the number of benzene rings decreases;<sup>1e</sup> *iv*) quantum efficiency also decreases as *n* decreases, so that while [*n*]CPPs with *n*  $\geq$  10 have high emission quantum yields (> 0.6) those with *n* = 5,6 do not emit at all.<sup>1e</sup>

The size-tunable properties of [*n*]CPPs make them attractive for several applications in optoelectronics. Understanding how chemical substituents can further affect the optoelectronic properties of those compounds, widening their field of potential applications, is still an almost unexplored field, with a few notable exceptions.<sup>5-7</sup> Recently,<sup>5</sup> Jasti and coworkers reported the synthesis of a 1,4-anthracene-incorporated [12]CPP, exploring its potential as intermediate to synthesize novel carbon materials.<sup>5</sup> Incorporation of strongly fluorescent groups into a [*n*]CPP skeleton could pave the way to obtain CPP-based optoelectronic materials with intriguing properties. Following this line, we report herein the synthesis and the optical properties of 9,10-anthracene-incorporated [8]CPP **2**.

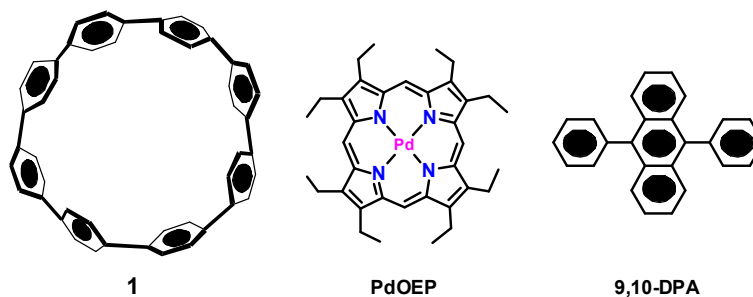
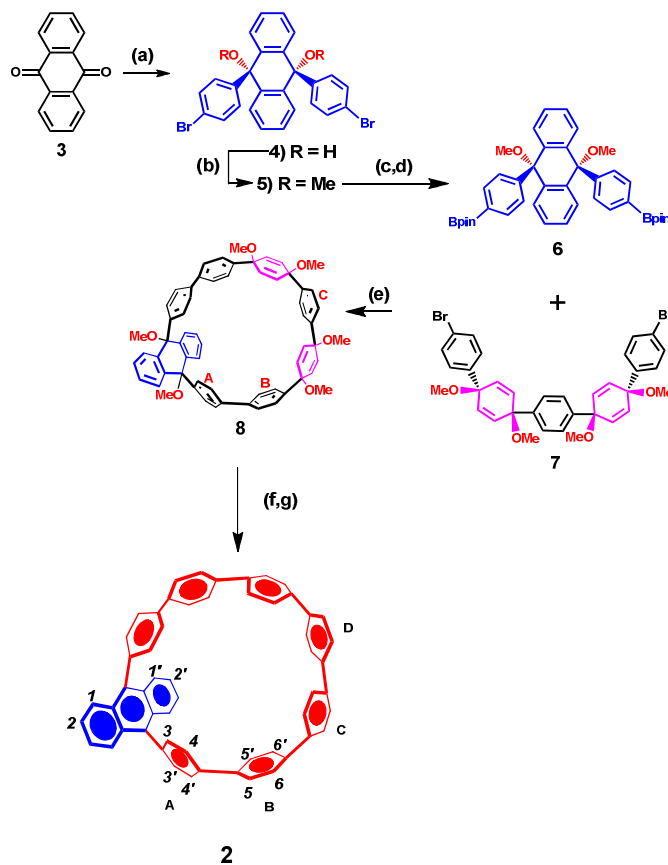


**Figure 1.** [8]Cycloparaphenylene **1**, palladium(II) octaethylporphyrin complex and 9,10-diphenylanthracene.

We show that this new compound exhibits unique optical properties with respect to its parent [8]CPP and affords bimolecular up-conversion (UC) of noncoherent,<sup>8</sup> low intensity light, in the presence of a proper sensitizer.<sup>8a</sup> This is an important process for converting low energy photons into light adequate for photovoltaic,<sup>9</sup> photocatalysis,<sup>10</sup> and bioimaging.<sup>11</sup> The most common method for triplet-triplet annihilation (TTA) UC involves the use of acceptor/annihilator molecules based on anthracene derivatives.<sup>12</sup> At this regard, the 9,10-DiPhenylAnthracene unit (DPA) (Figure 1) is a known acceptor in TTA photon UC processes.<sup>13</sup> Up-conversion abilities of 9,10-DPA-based nanoparticles have been exploited in lymph node in-vivo imaging in mouse,<sup>14</sup> while recently, it has been showed that 9,10-DPA also retains the up-conversion properties in supramolecular gels.<sup>15</sup> It is known that cycloparaphenylenes are excellent chromophores exhibiting high fluorescence quantum yields,<sup>1</sup> whereas, at the best of our knowledge, no literature data is available about their abilities as emitters into up-conversion schemes.



**Scheme 1.** Synthesis of **2**. (a) (4-Bromophenyl)lithium, THF,  $-78\text{ }^{\circ}\text{C}$ , 2 h. (b) NaH, MeI, dry THF,  $0\text{ }^{\circ}\text{C}$   $\rightarrow$   $25\text{ }^{\circ}\text{C}$ , 18 h. (c) *n*-BuLi, dry THF,  $-78\text{ }^{\circ}\text{C}$ . (d) isopropyl pinacol borate, 5 h. (e) Pd(OAc)<sub>2</sub>, S-Phos, K<sub>3</sub>PO<sub>4</sub>, DMF/H<sub>2</sub>O, 19 h,  $100\text{ }^{\circ}\text{C}$ . (f) Sodium Naphthalenide, dry THF,  $-78\text{ }^{\circ}\text{C}$ , 3 h. (g) I<sub>2</sub>, THF, 45 min.

Prompted by these consideration, we envisioned that the incorporation of a 9,10-DPA unit into a [8]CPP skeleton could afford the first example of a CPP-based emitter in photon up-conversion, thus widening the scope of this class of compounds. In the present work, we describe the synthesis of 9,10-DPA-incorporated [8]CPP macrocycle **2** (Scheme 1) and a study of its optoelectronic and up-conversion properties.

## RESULTS AND DISCUSSION

**Synthesis and NMR Characterization.** CPP derivatives are highly curved nanohoops in which the high strain of the macrocycle prevents the direct macrocyclization from linear paraphenylenes.<sup>1</sup> Consequently, Justi and coworkers<sup>1d</sup> reported a synthetic strategy which consists of a Suzuki-Miyaura cross-coupling/macrocyclization between rigidly-curved elements incorporating cyclohexa-2,5-diene moieties as masked benzene rings.<sup>1</sup> The precursor macrocycle thus obtained, is successively aromatized to CPP by reduction in the presence of sodium naphthalenide.<sup>1a</sup> On this basis, we have designed the synthesis of **2** by adapting the gram-scale protocol of Jasti and coworkers.<sup>1d</sup> In details, we have selected derivative **6** (Scheme 1), bearing the 9,10-dimethoxy-9,10-dihydroanthracene curved-moiety as a masked anthracene unit, to be coupled by Suzuki-Miyaura reaction with derivative **7**.<sup>1d</sup> The synthesis of **6** is outlined in Scheme 1. Anthraquinone **3** was reacted with (4-bromophenyl)lithium yielding the *syn*-diol **4**, in accordance with the electrostatic model proposed by Justi and coworkers.<sup>1c</sup> Successive deprotonation of **4** with sodium hydride in the presence of MeI afforded derivative **5**, which was converted in diboronate **6** by treatment with isopropyl pinacol borate. Derivative **6** underwent cyclization with **7** in the presence of Pd(OAc)<sub>2</sub>, S-Phos, and K<sub>3</sub>PO<sub>4</sub> in DMF/H<sub>2</sub>O, to give macrocycle **8**. This was confirmed by a HR MALDI-FT-ICR mass spectrum, which showed a molecular ion peak at *m/z* 894.3895 (Calcd. for C<sub>62</sub>H<sub>54</sub>O<sub>6</sub>, 894.3921). The <sup>1</sup>H NMR spectrum of **8** in CDCl<sub>3</sub> (600 MHz, 298 K) showed three OMe singlets at 3.46, 3.41, and 3.15 ppm, in a 1:1:1 ratio, which correlated in the HSQC spectrum (SI) with carbon signals at 52.0 and 52.2 ppm.

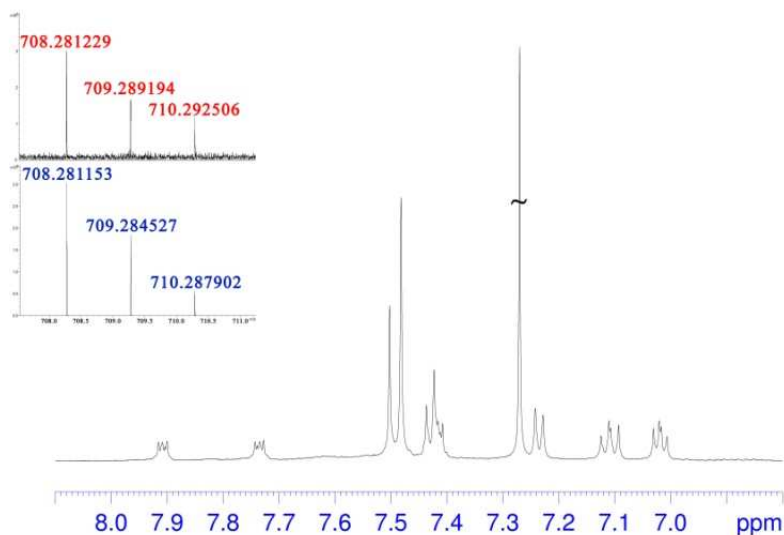


**Figure 2.** Significant portion of the  $^1\text{H}$  NMR spectrum of **2** (600 MHz,  $\text{CDCl}_3$ , 298 K). Inset: Significant portion of the isotope pattern in HR MALDI FT ICR mass spectrum of **2**, calculated (in blu) and experimental (in red).

Regarding the cyclohexadienyl moieties of **8**, an AB system was present at 6.03 and 6.11 ppm ( $J = 10.3$  Hz, 4H each), which correlated in the HSQC spectrum (SI) with two resonances at 133.0 and 133.5 ppm. In addition, the aromatic region of the  $^1\text{H}$  NMR spectrum of **8** evidenced the presence of two AB systems at 7.44/7.38 ppm ( $J = 8.5$  Hz, 4H each) and 7.17/6.92 ppm ( $J = 8.5$  Hz, 4H each) attributable to benzene rings A and B in Scheme 1. Finally, a singlet was present at 7.50 ppm attributable to ArH of ring C (4H). The  $^{13}\text{C}$  NMR spectrum of **8** evidenced the diagnostic presence of three singlets (DEPT-135) at 80.3, 74.6, and 74.3 ppm, attributable to the oxygenated carbon atoms.

The treatment of **8** with sodium naphthalenide at  $-78$  °C for 3 h in the dark, in degassed dry THF, followed by quenching with  $\text{I}_2$ , afforded [8]CPP **2** in 11 % yield. The HR MALDI-FT-ICR mass spectrum of **2** (inset of Figure 2) showed a molecular ion peak at  $m/z$  708.2812 (Calcd. for  $\text{C}_{56}\text{H}_{36}$ , 708.2811). A close inspection of the  $^1\text{H}$  NMR (Figure 2) and DQF-COSY spectra of **2** (SI) in  $\text{CDCl}_3$

(600 MHz, 298 K) revealed two distinct AA'BB' spin systems attributable to the aromatic hydrogen atoms 1/2 and 1'/2' (Scheme 1) of the anthracenyl group. In details, the two AA'BB' systems were detected at 7.89/7.39 and 7.72/7.41 ppm (DQF-COSY), and correlated in the HSQC spectrum with four distinct carbon resonances at 127.72, 128.64, 127.64, and 127.12 ppm, respectively.

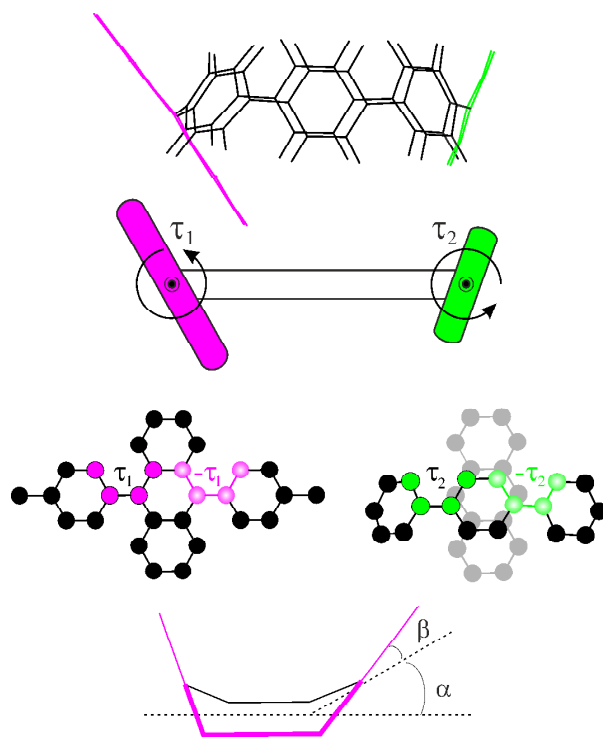


**Figure 3.** Schematic representation of **2** indicating the dihedral angles  $\tau_1$  and  $\tau_2$  and the deformation and bent angles  $\alpha$  and  $\beta$ .

This result clearly indicates that the two peripheral benzene rings of the anthracenyl group in **2** are nonequivalent because of their different *in/out* orientation with respect to the CPP cavity, which implies a hindered rotation around  $\tau_1$  (Figure 3). Because of this restricted rotation, the benzene ring A, adjacent to the anthracenyl group, adopts an inclined orientation, and the two 3/3' (and 4/4') protons (Scheme 1) become nonequivalent. Consequently, in the  $^1\text{H}$  NMR spectrum of **2** (SI) two AB systems were detected for the *ortho*-coupled 3/4 and 3'/4' (Scheme 1) protons at 7.11/7.01 ( $J = 6.1$  Hz, 4H) and

7.00/7.08 ppm ( $J = 9.0$  Hz, 4H). VT  $^1\text{H}$  NMR experiments (400 MHz,  $\text{C}_2\text{D}_2\text{Cl}_4$ ) evidenced no hint of coalescence up to 493 K for the 1/1', 2/2', 3/3', and 4/4' protons. In addition, the  $^1\text{H}$  NMR and DQF-COSY spectra of **2** evidenced the presence of an AB system at 7.42/7.23 ppm ( $J = 8.4$  Hz, 8H) attributable to 5/6 H-atoms of ring B (Scheme 1). In fact, because of the fast (with respect to the NMR time scale) rotation around the C-C bond connecting A and B rings, the protons 5 and 5' (and 6/6') become equivalent. Finally, the ArH of rings C and D resonate as two sharp singlets at 7.47 and 7.49 ppm in 2:1 ratio (Figure 2).

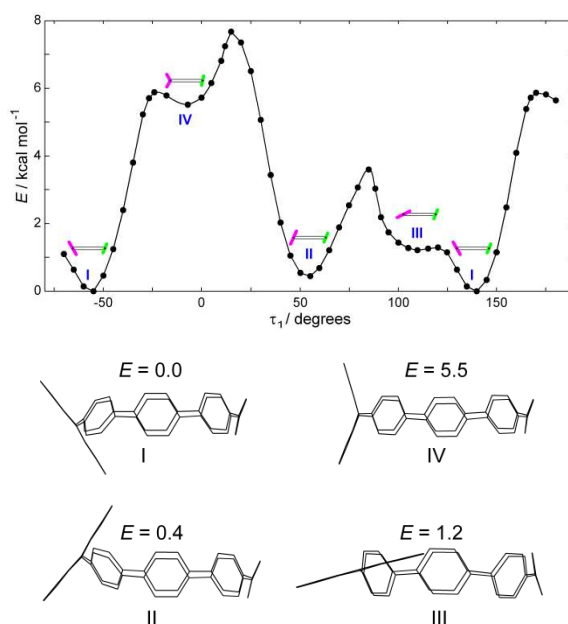


**Figure 4.** (Top) Potential energy profile (PCM/B97D/TZVP) of **2** along the  $\tau_1$  coordinate. Energy is referred to the most stable conformer **I**. (bottom) The most stable conformers of **2** and their relative energies ( $E / \text{kcal mol}^{-1}$ ).

**Structural and optoelectronic properties.** Since the NMR spectra of **2** suggest the occurrence of a plane of symmetry, geometry optimizations of **2** were initially restricted to the  $C_s$  point group. To that

end, we computed the optimized potential energy profile along the Lagrangian variable  $\tau_1$  (Figure 3), by fixing in each step the two dependent dihedral angles and performing a full optimization of all the other nuclear coordinates.

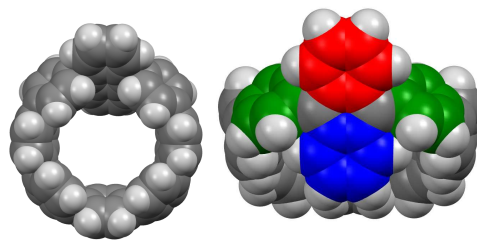


**Figure 5.** Different views of the optimized structure (DFT calculations, PCM/B97D/TZVP) of **2** (I in Figures 4).

The resulting potential energy profile is reported in Figure 4 (top); four minimum energy structures (I-IV in Figure 4, bottom) have been found, the most relevant of which fall within an energy range of ca 1 kcal/mol. The statistically relevant conformers at room temperature are all characterized by an alternating zig-zag conformation of the phenylene rings, the dihedral angle between neighboring phenylene units being ca 28 degrees, close to the optimal value of 30° found for  $[n]$ CPP systems.<sup>1,16</sup>

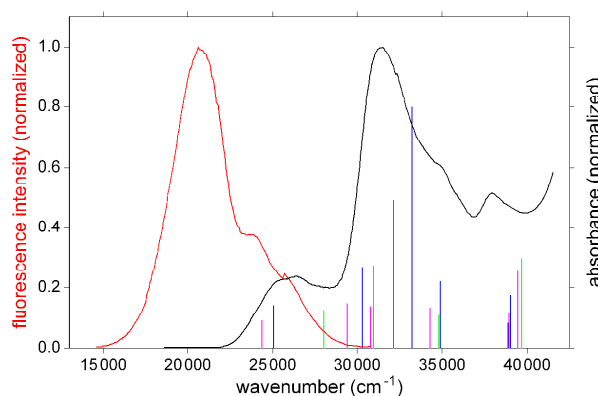


**Figure 6.** Normalized UV/vis absorption (black) and emission (red) spectra of **2** in  $\text{CH}_2\text{Cl}_2$  and computed (PCM/TDCAM-B3LYP/6-31+G\*\*) vertical electronic transitions (vertical lines) of conformers I (blue), II (violet), and III (green).

1  
2  
3 The dihedral angle  $\tau_1$  is roughly  $60^\circ$  in both conformers I and II, reaching the expected value for free  
4  
5 9,10 DPA ( $\approx 77^\circ$ ) only in III. Different stereochemical views of the optimized structure  
6  
7 (PCM/B97D/TZVP) of the most stable conformer of **2** are shown in Figure 5. Deformation and bent  
8  
9 angles ( $\alpha$  and  $\beta$  in Figure 3) amount to  $6.2^\circ$  and  $14.2^\circ$ , respectively, close to the values of  $9.3^\circ$  and  $13.7^\circ$   
10  
11 observed for  $\alpha$  and  $\beta$  in the phenyl rings of [8]CPP. These indicate that the steric hindrances between the  
12  
13 two peripheral benzene rings (1 and 1' positions in Scheme 1) of the 9,10-DPA core and the adjacent  
14  
15 phenyl rings causes a substantial distortion of the central unit of the anthracene ring, as already found in  
16  
17 1,4-anthracene incorporated [12]CPP's.<sup>5</sup> To ascertain that all the relevant conformations have been  
18  
19 actually located, we have also carried out: *i*) geometry optimizations by scanning the  $\tau_2$  variable of  
20  
21 Figure 3 (SI), and *ii*) geometry optimizations starting from random conformations generated either  
22  
23 preserving or relaxing the  $C_s$  symmetry. No additional minimum energy conformations were found.  
24  
25 Cyclic voltammetry measurements showed that the first oxidation peak of **2** is quasi-reversible (SI), with  
26  
27 a half wave potential falling at 0.53 V vs  $\text{Fc}^+/\text{Fc}$  redox couple, similar to that found for [8]CPP (0.59  
28  
29 V),<sup>1</sup> but significantly different from that of 1,4-anthracene-incorporated [12]CPP (0.65 V).<sup>5</sup> The first  
30  
31 oxidation potential of the most stable conformer (I, SI) is predicted to be at +0.52 V vs  $\text{Fc}^+/\text{Fc}$  by  
32  
33 (RO)CAM-B3LYP computations, in excellent agreement with the experimental value. Mulliken spin  
34  
35 density analysis shows that the hole in the radical cation  $\mathbf{2}^{+\bullet}$  is mainly, but not fully (80%), localized on  
36  
37 the anthracene moiety, in line with previous results reported for the 1,4-anthracene-incorporated  
38  
39 [12]CPP derivative (1,4-DPA-[12]CPP).<sup>5</sup> Indeed, DFT calculations at PCM-CAM-B3LYP/6-31+G\*\*  
40  
41 level predict that the HOMO and LUMO of **2** are mainly localized on the anthracene moiety (Figure 6).  
42  
43 The predicted HOMO/LUMO energy gap of **2** is 2.2 eV, significantly lower than that calculated for 1,4-  
44  
45 DPA-[12]CPP derivative (3.06 eV).<sup>5</sup> The absorption and the emission spectra of **2** are reported in Figure  
46  
47 6. The absorption spectrum is characterized by an intense band peaked at 320 nm ( $\epsilon = 1.7 \times 10^4 \text{ M}^{-1}$   
48  
49  $\text{cm}^{-1}$ ) and by a less intense absorption extending from 360 to 450 nm. The former signal is characteristic  
50  
51  
52  
53  
54  
55  
56  
57  
58  
59  
60

of  $[n]$ CPP systems, while the latter resembles very closely that of 9,10-DPA, even though it lacks of its peculiar vibronic structure.

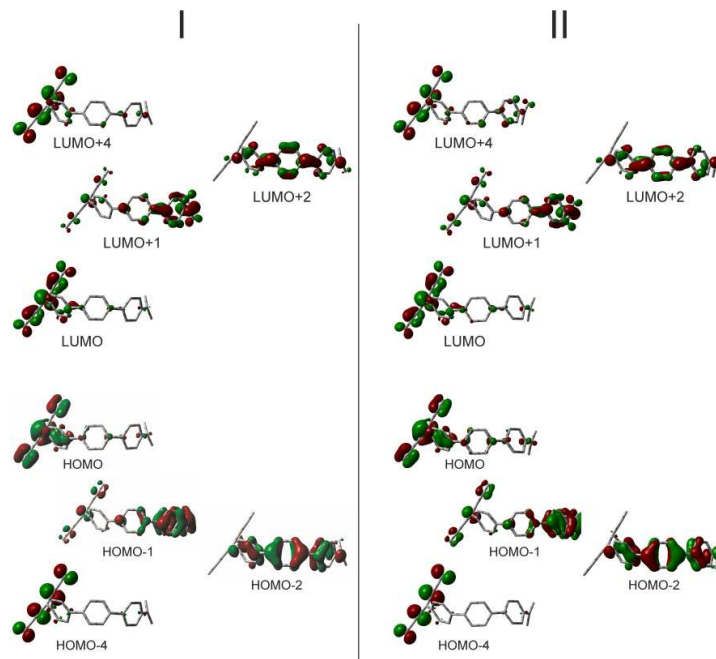


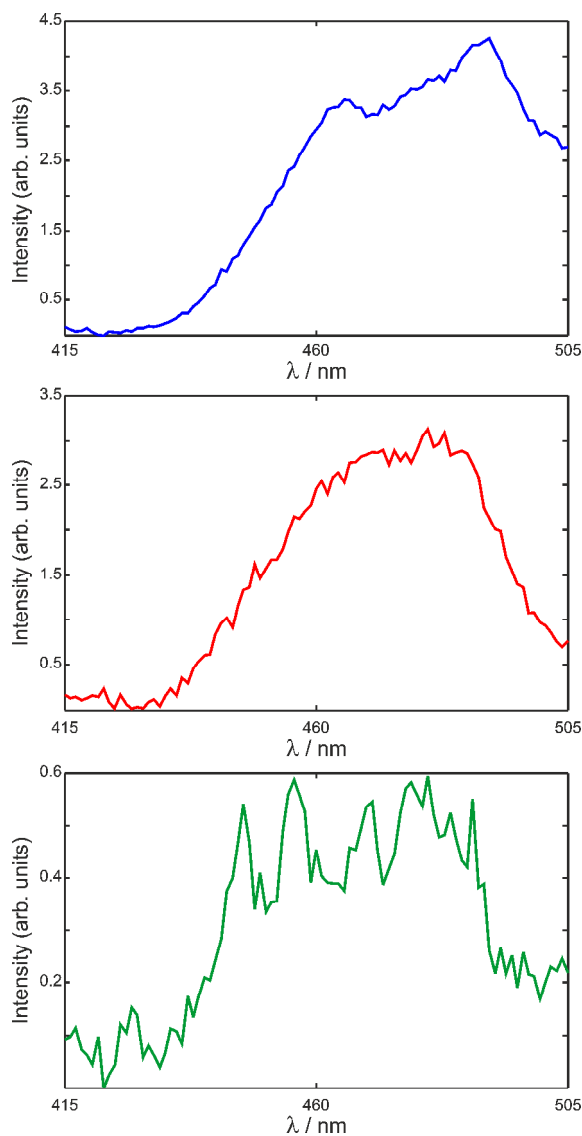
**Figure 7.** Isodensity surface plots of the frontier Kohn-Sham orbitals of the most populated conformers of **2**.

On the whole, the absorption spectrum of **2** is mainly given by the superposition of the signals of isolated 9,10-DPA and  $[8]$ CPP, suggesting that the two molecular moieties maintain in the ground state their own electronic structure, at least as concerns frontier orbitals. The above hypothesis has been checked by theoretical calculations carried out at PCM/TDCAM-B3LYP/6-31+G\*\* level of theory. Predicted lowest energy transitions are reported in Table S1 and sketched in Figure 6, where the computed transition strengths, averaged over Boltzmann conformer populations, are reported as a function of the absorption wavelength and are superimposed to the experimental UV/vis spectrum. Computed optical transitions agree well with the observed absorption spectrum. The broad spectral

absorption observed in the region 350-450 nm corresponds to the absorptions predicted at 400, 410, and 380 nm for conformers I, II, and III, respectively (Table S1). The lower symmetry of **2** with respect to unsubstituted [8]CPP, reflects in a reduced  $\sigma$ - $\pi$  orbital mixing which makes the HOMO-LUMO absorption, symmetry forbidden in [8]CPP, a bright transition ( $f \approx 0.3$ , see Table S1).<sup>17</sup> The  $S_1 \leftarrow S_0$  transitions predicted at ca 400 nm (Table S1) result from the excitation of one electron from the HOMO to the LUMO, which are both Kohn-Sham  $\pi$  orbitals localized over the 9,10-DPA moiety, as shown in Figure 7. The electronic transitions, which are predicted to fall between 290 and 340 nm, are reported in Table S1 for the three low energy conformers; the involved Kohn-Sham orbitals are sketched in Figure 7 for the two most populated conformers. For conformer I, there are two transitions with significantly higher electric dipole transition moments, falling at 330 and 301 nm. The former transition mainly consists of HOMO-1  $\rightarrow$  LUMO+1 electron excitation, both levels being mainly localized on the five phenyl rings of CPP which do not belong to DPA, so that electron density changes upon excitation does not significantly involve the DPA moiety, see Figure 7. The transition at 301 nm mainly consists of HOMO-2  $\rightarrow$  LUMO+1 and HOMO-1  $\rightarrow$  LUMO+2 electron excitations. The HOMO-2 and LUMO+2 are mainly localized on the six phenylene rings surrounding the DPA moiety and the opposite phenyl ring, thus also this transition does not involve the DPA moiety. The same holds true also for conformers II and III.<sup>18,19,1e,20</sup>

The fluorescence spectrum of **2** is broad, extending from 350 up to 650 nm, with a peak at 485 nm. The slightly structured signal occurring at shorter wavelengths, see Figure 6, is somewhat characteristic of the 9,10-DPA unit, whose emission spectrum in cyclohexane is characterized by vibronic peaks in the region 400-450 nm.<sup>21</sup> By contrast, the emission peak is significantly blue-shifted with respect to that of [8]CPP, whose emission spectrum is peaked at ca. 530 nm,<sup>1e</sup> being more similar to those of [n]CPP hoops, with  $n > 9$ . It is known that [n]CPPs exhibit a large increase in fluorescence quantum efficiencies ( $\Phi$ ) for increasing value of  $n$ , for [16]CPP  $\Phi=0.9$  while for [8]CPP  $\Phi=0.1$ . The fluorescence quantum yield of **2** has been measured by using the relative method reported by Miller and co-workers.<sup>22</sup> Using quinine sulphate as standard, the fluorescence quantum yield of **2** is  $\Phi = 0.47$ , which is significantly

1 higher than that observed for [8]CPP and closer to the values observed for larger [9-12]CPP  
2 derivatives.<sup>1e</sup> Summarizing, both the emission spectrum and the result of quantum yield measurements  
3 reveal that the emission properties of **2** are more similar to that of nanohoops of higher dimensions.  
4 According to TDDFT computations, the electronic excitations of **2** involve Kohn-Sham orbitals which  
5 are mainly localized either on the 9,10-DPA moiety or on the remaining five CPP rings (Figure 7). The  
6 formation of an excitonic state localized on five phenylene rings, which characterizes the excited state  
7 geometries of [n]CPPs with  $n > 8$ ,<sup>16</sup> can also likely occur in **2**, making its emission properties more  
8 similar to those of higher size nanohoops.  
9  
10  
11  
12  
13  
14  
15  
16  
17  
18  
19  
20

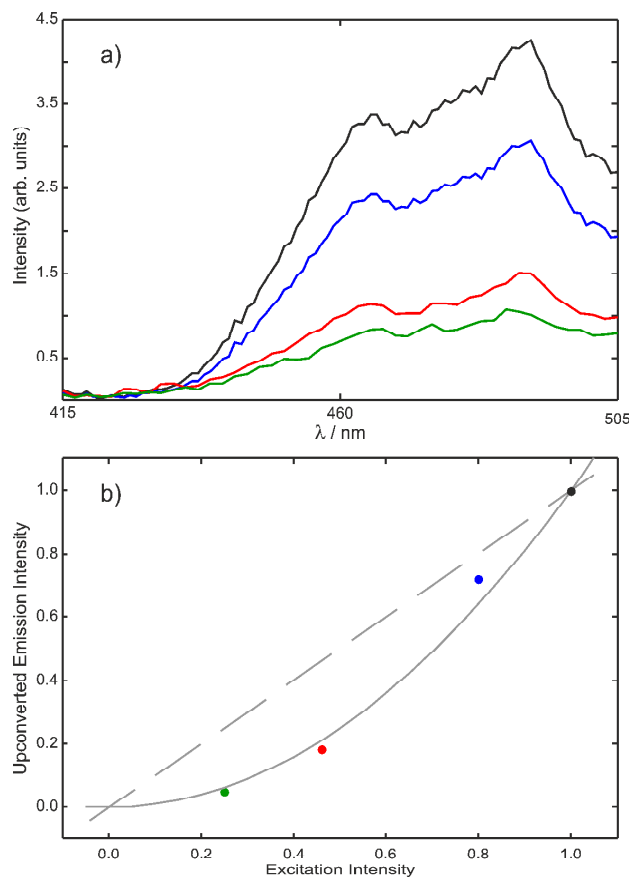


1 **Figure 8.** Upconverted emission spectra of **2** (1 mM) and PdOEP in CH<sub>2</sub>Cl<sub>2</sub>,  $\lambda_{\text{exc}} = 540$  nm. Blue:  
2 [PdOEP]= 10  $\mu$ M; red: [PdOEP]= 100  $\mu$ M; green: [PdOEP]= 1.0 mM. Light source was passed through  
3 a 295 nm long pass cut-off emission filter prior to incidence on samples.  
4  
5  
6  
7  
8  
9

10 9,10-DPA (Figure 1) has been already successfully used as emitter in upconversion of non-coherent  
11 light of low intensity, in the presence of a phosphorescent molecule, usually Pd or Pt complexes.<sup>8a</sup> The  
12 peculiar properties of **2**, which retains most of spectral features of 9,10-DPA, could indeed make it a  
13 potential emitter in low intensity upconversion process. We have thus investigated the optical response  
14 of **2** in DCM solution, employing as sensitizer palladium(II) octaethylporphyrin (PdOEP). A few  
15 solutions of **2** and PdOEP at different concentration ratios were prepared in anhydrous CH<sub>2</sub>Cl<sub>2</sub> under  
16 nitrogen atmosphere and then transferred into a quartz cuvette and sealed. Excitation of PdOEP at 540  
17 nm produced the anti-Stokes emissions shown in Figure 8. The shape of the upconverted emission  
18 depends on the concentration of the sensitizer, because of the partial overlap with the absorption  
19 spectrum of PdOEP. Indeed, at low [PDOEP]/[CPP] concentration ratios the emission profile is much  
20 more similar to the normal excitation spectrum, cfr. Figure 6. The slight shoulder appearing at 460 nm  
21 is reasonably due to partial reabsorption by the sensitizer in the region 470-520 nm, see Figure S20 of  
22 S.I., as also confirmed by the fact that at higher concentration ratios the peak at longer wavelength  
23 disappears and the emission band appears flat in the region 460-490 nm, see figure 8. The emission  
24 spectrum obtained by up-conversion is significantly red shifted with respect to that previously reported  
25 for 9,10-DPA,<sup>8a</sup> demonstrating that emission involves the first excited state of the whole nano-hoop.  
26  
27  
28  
29  
30  
31  
32  
33  
34  
35  
36  
37  
38  
39  
40  
41  
42  
43  
44  
45  
46

47 Reasonably, the anti-Stokes emission at  $\lambda_{\text{exc}} = 540$  nm takes place via sensitized TTA process. As first  
48 pointed out by Parker and Hatchard and deeper investigated by Castellano and coworkers,<sup>23</sup> light  
49 upconversion occurring via TTA is characterized, at least at low power density of the incident light, by  
50 a quadratic dependence of the emission intensity upon the power of the incident light. To have a better  
51 mechanistic insight of the observed anti-Stokes fluorescence, we have investigated the dependence of  
52  
53  
54  
55  
56  
57  
58  
59  
60

1 the emission signal upon excitation light power in the region of low power density. The results are  
2 presented in Figure 9, where the upconverted emissions of a solution of **2** (0.5 mM) and PdOEP (10  $\mu$ M)  
3 in anhydrous  $\text{CH}_2\text{Cl}_2$  prepared under nitrogen atmosphere and irradiated at different incident power  
4 densities (maximum power density  $\approx 0.8\text{mW}/\text{cm}^2$ ) are shown.  
5  
6  
7  
8  
9  
10  
11  
12  
13  
14  
15  
16  
17  
18  
19  
20  
21  
22  
23  
24  
25



26  
27  
28  
29  
30  
31  
32  
33  
34  
35  
36  
37  
38  
39  
40  
41  
42  
43 **Figure 9.** Upconverted emission intensity profiles of a solution of **2** (0.5mM) and PdOEP (10  $\mu$ M) in  
44 dichloromethane at different incident power density (top) and the corresponding normalized integrated  
45 emission as a function of the normalized incident power bottom. Dashed line  $y=x$ , full line  $y=x^2$ ;  
46 maximum incident power  $0.8\text{ mWcm}^{-2}$ .  
47  
48  
49  
50  
51  
52  
53  
54  
55  
56  
57  
58  
59  
60

1  
2  
3 The emission band shape is independent of the excitation power. In Figure 9b, the integrated emission  
4 intensities of Figure 9a is reported as a function of the power density of the incident light, both  
5 normalized at their highest values. Figure 9b clearly indicates that the emission intensity depends on the  
6 square of the power of the incident light, in agreement with previous studies,<sup>23b,c</sup> thus confirming that  
7 the upconversion occurs via sensitized TTA.  
8  
9  
10  
11  
12

## 13 14 15 16 **Conclusions**

17  
18  
19 9,10 anthracene-incorporated [8]cycloparaphenylene has been synthesized adapting the gram-scale  
20 synthesis recently reported by Jasti. The compound has been characterized by HR MALDI mass  
21 spectroscopy and 1D and 2D NMR spectroscopy, evidencing a Cs symmetry. The absorption spectrum  
22 is characterized by two low energy transitions, one at longer wavelength, attributable to the 9,10-DPA,  
23 the other falling at wavelengths characteristic of [n]CPP systems. The emission spectrum is however  
24 significantly different from [8]CPP one, better resembling that of larger size nano-hoops, both for the  
25 peak wavelength and quantum yield. In the presence of the octaethylporphyrin Pd(II) complex as  
26 sensitizer, 9,10-anthracene-incorporated [8]CPP undergoes visible light upconversion, the first case  
27 reported in the literature in which a cycloparaphenylene derivative is involved as emitter in low power  
28 light frequency conversion.  
29  
30  
31  
32  
33  
34  
35  
36  
37  
38  
39  
40  
41  
42  
43

## 44 **Experimental Section**

45  
46 **General Information.** HR MALDI mass spectra were recorded on a FT-ICR mass spectrometer  
47 equipped with a 7T magnet. The samples were ionized in positive ion mode using ESI positive mode  
48 and MALDI ion source. The mass spectra were calibrated externally, and a linear calibration was  
49 applied. The samples recorded in MALDI were prepared by mixing 10  $\mu$ L of analyte in dichloromethane  
50 (1 mg/mL) with 10  $\mu$ L of solution of dithranol (10 mg/mL in THF). Tetrahydrofuran was dried by  
51 heating under reflux over sodium wire in the presence of benzophenone as indicator while  
52  
53  
54  
55  
56  
57  
58  
59  
60

1 dimethylformamide were dried by activated 3 Å molecular sieves. All chemicals reagents grade were  
2 used without further purification and were used as purchased. Derivative **7**<sup>1d</sup> and sodium naphthalenide<sup>1a</sup>  
3 were prepared in accord to reported procedures.<sup>1d</sup> Reaction temperatures were measured externally.  
4  
5 Reactions were monitored by TLC silica gel plates (0.25 mm) and visualized by UV light 254 nm, or by  
6  
7 spraying with H<sub>2</sub>SO<sub>4</sub>-Ce(SO<sub>4</sub>)<sub>2</sub>. NMR spectra were recorded on a 600 [600 (<sup>1</sup>H) and 150 MHz (<sup>13</sup>C)],  
8  
9 400 [400 (<sup>1</sup>H) and 100 MHz (<sup>13</sup>C)], 300 MHz [300 (<sup>1</sup>H) and 75 MHz (<sup>13</sup>C)] or 250 MHz [250 (<sup>1</sup>H) and  
10  
11 62.5 MHz (<sup>13</sup>C)] spectrometer. Chemical shifts are reported relative to the residual solvent peak.  
12  
13  
14  
15  
16  
17

18 **Computational details.** Constrained and unconstrained geometry optimizations were carried at the  
19 density functional level of theory (DFT), by using the B97D functional including the empirical  
20 correction for dispersion energy proposed by Grimme,<sup>24</sup> in conjunction with the density fitting  
21 approximation and the TZVP basis set. The nature of the stationary points was verified by computing  
22 the eigenvalues of the Hessian matrix. B97D was chosen because it has been proven to be the most  
23 accurate method in predicting torsional barriers of substituted biphenyls.<sup>25</sup> Time dependent (TD) DFT  
24 computations were carried out by using the CAM-B3LYP range-separated hybrid functional.<sup>26</sup> Indeed, it  
25 is well known that electronic excitations in conjugated oligomers have a charge transfer nature, with  
26 structural distortions that can be modelled only with the use of range-corrected hybrid DFT models  
27 including long range electronic exchange interactions<sup>16,27</sup> The same functional was adopted for the  
28 computation of the first oxidation potential. The restricted open shell (RO) formalism was used because  
29 it yields more accurate oxidation potentials when used with the CAM-B3LYP functional. The absolute  
30 potential of Fc<sup>+</sup>/Fc in dichloromethane has been set to 4.98 V.<sup>28</sup> The 6-31+G(d,p) basis set was adopted  
31 for all the computations employing the CAM-B3LYP functional. Effects due to solvent  
32 (dichloromethane) polarization were included in all computations by the polarizable continuum model  
33 (PCM).<sup>29</sup> DFT and TDDFT computations were carried out by using the Gaussian program.<sup>30</sup>  
34  
35  
36  
37  
38  
39  
40  
41  
42  
43  
44  
45  
46  
47  
48  
49  
50  
51  
52  
53  
54

55 **Optoelectronic characterization.** Optical absorption spectra were measured on a Cary 50 UV-vis  
56 spectrophotometer from Varian. Steady-state luminescence spectra were recorded on a modular  
57  
58  
59  
60

1 fluorescence spectrometer from Acton Research, equipped with a xenon lamp. Light source was passed  
2 through a 295 nm long pass cut-off emission filter prior to incidence on the sample. All solution samples  
3 were deaerated with nitrogen. Relative quantum yields of **2** in dichloromethane were determined as  
4 described by Williams using quinine sulfate (0.1 M H<sub>2</sub>SO<sub>4</sub>) as standard. Excitation occurred at 319 nm  
5 and the fluorescence of **2** was integrated from 350 – 650 nm, both for **2** and for quinine sulphate. In up-  
6 conversion measurements an additional longpass filter cutting at ca. 300 nm has been employed to  
7 completely cut down possible emission produced by excitation of second order diffraction. The quantum  
8 yield measurements were performed in accord with the method reported by Miller and co-workers.<sup>23</sup> The  
9 CPP **2** solutions were diluted to give absorbance values in the range 0.02-0.35, within the expected  
10 linear calibration range of fluorescence emission versus concentration. The quantum yields were  
11 calculated according to equation reported by Miller.

$$\Phi_X = \Phi_R \frac{I_X A_R \eta_X^2}{I_R A_X \eta_R^2}$$

12  $\Phi_R$  is the quantum yield of the standard,  $A$  is the absorbance of the solution,  $I$  is the integrated  
13 intensity of the exciting light and  $\eta$  is the average refractive index of the solution. Subscripts R and X  
14 refer to the reference and unknown compound, respectively. Cyclic voltammetry measurements were  
15 performed in CH<sub>2</sub>Cl<sub>2</sub> with TBAP as electrolyte. All potentials were referenced to the platinum quasi-  
16 reference electrode. The potential has been calibrated with ferrocene/ferrocenium (Fc/Fc<sup>+</sup>) redox couple.

17  
18  
19  
20  
21  
22  
23  
24  
25  
26  
27  
28  
29  
30  
31  
32  
33  
34  
35  
36  
37  
38  
39  
40  
41  
42  
43  
44 **Derivative 5.** 1,4-Dibromobenzene (10.0 g, 42.4 mmol) was dissolved in 450 mL of dry THF and  
45 cooled to -78 °C. To this solution was added a 2.5 M solution of *n*-butyllithium in *n*-hexane (18.2 mL,  
46 45.5 mmol) over 15 min and the reaction mixture was stirred for 30 min. Anthraquinone (4.31 g, 20.7  
47 mmol) was added to the reaction mixture in three equal portions over 30 min. The solution was stirred  
48 for 2 h at -78 °C and then added to 180 mL of water. The mixture was further diluted by the addition of  
49 180 mL of diethyl ether and the organic layer was separated. The aqueous layer was extracted with  
50 diethyl ether (3 x 70 mL) and the combined organic layers were washed with a saturated brine solution  
51  
52  
53  
54  
55  
56  
57  
58  
59  
60

(100 mL). The organic phase was then dried over sodium sulfate, filtered and evaporated under reduced pressure to give the diol product **4** which was used without further purification. The diol **4** was dissolved in 70 mL of dry THF and sodium hydride (2.07 g, 51.7 mmol, 60% in mineral oil) was added at 0 °C. The mixture was stirred for 30 min and methyl iodide (5.2 mL, 83 mmol) was added. The mixture was allowed to warm to room temperature and stirred for an additional 18 h. The excess of sodium hydride was then quenched by addition of 100 mL of water and filtered. The white solid was washed with 120 mL of ethyl ether and dried in vacuum for 12 h, to give **5** in 53% of yield (6.04 g). M. p. > 310 °C dec. <sup>1</sup>H NMR (400 MHz, 298 K, CDCl<sub>3</sub>): δ (ppm) 7.49 (m, 4H, Ar-H), 7.30 - 7.33 (overlapped, 8H, Ar-H), 7.19 (d, *J* = 8.5 Hz, 4H, Ar-H), 2.93 (s, 6H, OMe); <sup>13</sup>C NMR (100 MHz, CDCl<sub>3</sub>): δ (ppm) 147.9, 138.2, 131.0, 128.7, 128.2, 121.1, 78.7, 51.3. HRMS (ESI+): *m/z* [M+Na]<sup>+</sup> calculated for C<sub>28</sub>H<sub>22</sub>Br<sub>2</sub>NaO<sub>2</sub>: 572.9864, found 572.9859.

**Derivative 6. 5** (2.53 g, 4.77 mmol) was dissolved in 280 mL of dry THF and cooled to -78 °C. Then a 2.5 M solution of *n*-butyllithium in hexane (9 mL, 22.5 mmol) was added over 10 min. Then isopropyl pinacol borate (8.50 mL, 42.0 mmol) was added rapidly and the solution was stirred for 5 h under argon. 200 mL of water and 100 mL of ethyl acetate were added to the solution and the biphasic mixture was stirred for 30 min at room temperature. The organic phase was extracted and the aqueous layer was washed with ethyl acetate (3 x 70 mL). The combined organic layers were dried over sodium sulfate, filtered and concentrated in vacuum to give a colorless oil that was purified by chromatography on silica gel (hexane/ethyl acetate, 7:3). The product **6** was obtained as a white solid in 41% of yield (1.30 g). M.p.: 252.2-253.3°C. <sup>1</sup>H NMR (400 MHz, 298 K, CDCl<sub>3</sub>): δ (ppm) 7.68 (d, *J* = 8.1 Hz, 4H, Ar-H), 7.48 (m, 4H, Ar-H), 7.43 (d, *J* = 8.1 Hz, 4H, Ar-H), 7.24 (m, 4H, Ar-H), 2.94 (s, 6H, OMe), 1.30 (s, 24H, CH<sub>3</sub>); <sup>13</sup>C NMR (62.5 MHz, CDCl<sub>3</sub>): δ (ppm) 152.1, 138.5, 134.5, 128.5, 128.4, 126.2, 83.8, 79.0, 51.2, 25.0. HRMS (ESI+): *m/z* [M+Na]<sup>+</sup> calculated for C<sub>40</sub>H<sub>46</sub>B<sub>2</sub>NaO<sub>6</sub>: 667.3378, found 667.3380.

**Derivative 8.** Dibromide **7** (1.99 g, 3.00 mmol), diboronate **6** (1.93 g, 3.00 mmol), S-Phos (246 mg, 0.61 mmol) and K<sub>3</sub>PO<sub>4</sub> (2.55 g, 12.0 mmol) in a mixture of DMF/H<sub>2</sub>O (600 mL/60mL) was mixed and degassed twice through freeze/pump/thaw technique. Then Pd(OAc)<sub>2</sub> (471 mg, 2.11 mmol) was added

1 and the mixture was stirred at 100 °C for 19 h under argon. After cooling to room temperature, the  
2 mixture was filtered through a short plug of Celite® and added to 150 mL of water and 100 mL of  
3 CHCl<sub>3</sub>. The biphasic mixture was stirred for 30 min and separated. The aqueous layer was washed with  
4 CHCl<sub>3</sub>. The biphasic mixture was stirred for 30 min and separated. The aqueous layer was washed with  
5 CHCl<sub>3</sub> (3 x 80 mL). The combined organic layers were washed with 200 mL of a saturated brine  
6 solution and dried over sodium sulfate. After filtration the solvent was evaporated under vacuum, the  
7 crude mixture was purified by column chromatography on silica gel (Hexane/CH<sub>2</sub>Cl<sub>2</sub>/Et<sub>2</sub>O = 29:70:1) to  
8 give the macrocycle **8** as a white solid in 10 % of yield (0.27 g). M. p. > 305 °C dec. <sup>1</sup>H NMR (600  
9 MHz, 298 K, CDCl<sub>3</sub>): δ (ppm) 7.85 (m, 4H, Ar-H), 7.50 (s, 4H, Ar), 7.47 (m, 4H, Ar-H), 7.44 (d, *J* =  
10 8.5 Hz, 4H, CH=CH), 7.38 (d, *J* = 8.5 Hz, 4H, CH=CH), 7.17 (d, *J* = 8.5 Hz, 4H, CH=CH), 6.92 (d, *J* =  
11 8.5 Hz, 4H, CH=CH), 6.11 (d, *J* = 10.3 Hz, 4H, CH=CH), 6.03 (d, *J* = 10.3 Hz, 4H, CH=CH), 3.46 (s,  
12 6H, OMe), 3.41 (s, 6H, OMe), 3.15 (s, 6H, OMe). <sup>13</sup>C NMR (150 MHz, 298 K, CDCl<sub>3</sub>): δ (ppm) 145.0,  
13 143.4, 142.8, 139.8, 139.5, 138.6, 133.5, 133.0, 128.3, 127.5, 126.9, 126.3, 126.1, 80.3, 74.6, 74.3, 52.2,  
14 52.0. DEPT-135 (150 MHz, CDCl<sub>3</sub>): δ (ppm) 133.5, 133.0, 128.3, 127.5, 126.9, 126.3, 126.1, 52.2,  
15 52.0. HRMS (MALDI): *m/z* M<sup>+</sup> calculated for C<sub>62</sub>H<sub>54</sub>O<sub>6</sub>: 894.3921, found 894.3895.

16  
17  
18  
19  
20  
21  
22  
23  
24  
25  
26  
27  
28  
29  
30  
31  
32  
33  
34 **Derivative 2.** Derivative **8** (225 mg, 0.25 mmol) was dissolved in 18 mL of dry THF, under argon,  
35 and the solution was degassed through freeze/pump/thaw technique and cooled to -78 °C. Then, a  
36 solution of sodium naphthalenide in dry THF, freshly prepared (2.7 mL, 2.7 mmol) was added and the  
37 reaction mixture was stirred for 3 h at -78 °C. Then I<sub>2</sub> was added (3 mL of a 1.0 M solution in THF) and  
38 the reaction mixture was warmed at room temperature. Subsequently a saturated solution of sodium  
39 thiosulfate (50 mL) and CHCl<sub>3</sub> (50 mL) were added, and the reaction mixture was stirred for 10 min.  
40 The organic layer was extracted and the aqueous phase was washed with CHCl<sub>3</sub> (3 x 50 mL) and finally  
41 the combined organic layers was washed with a saturated brine solution (60 mL) and dried over sodium  
42 sulfate and filtered. The solvent was removed under reduced pressure, and the crude product was  
43 purified by chromatography column on silica gel under nitrogen flow (*n*-hexane/CH<sub>2</sub>Cl<sub>2</sub> = 3:7), to give  
44 the product **2** as a yellow solid in 11 % of yield (19 mg). M. p. > 285 °C dec. <sup>1</sup>H NMR (600 MHz, 298  
45  
46  
47  
48  
49  
50  
51  
52  
53  
54  
55  
56  
57  
58  
59  
60

1 K, CDCl<sub>3</sub>):  $\delta$  (ppm) 7.89 (m, 2H, Ar-H), 7.72 (m, 2H, Ar-H), 7.49 (s, 4H, Ar-H), 7.47 (s, 8H, Ar-H),  
2 7.42-7.40 (overlapped, 8H, Ar-H), 7.22 (d,  $J = 8.3$  Hz, 4H, Ar-H), 7.11-7.08 (overlapped, 4H, Ar-H),  
3 7.02-7.00 (overlapped, 4H, Ar-H). <sup>13</sup>C NMR (150 MHz, CDCl<sub>3</sub>):  $\delta$  (ppm) 146.6, 146.5, 142.7, 140.3,  
4 139.7, 138.8, 138.4, 137.2, 137.0, 136.9, 128.6, 128.3, 128.0, 127.9, 127.8, 127.7, 127.6, 127.5, 127.5,  
5 127.4, 127.2, 127.1, 127.1. DEPT-135 (150 MHz, CDCl<sub>3</sub>):  $\delta$  (ppm) 128.6, 128.3, 128.0, 127.9, 127.8,  
6 127.7, 127.6, 127.5, 127.5, 127.4, 127.2, 127.10, 127.12. HRMS (MALDI):  $m/z$  M<sup>+</sup> calculated for  
7 C<sub>56</sub>H<sub>36</sub>: 708.2811, found 708.2812.  
8  
9  
10  
11  
12  
13  
14  
15  
16  
17

## 18 Acknowledgements

19  
20  
21 The authors acknowledge the Regione Campania (POR CAMPANIA FESR 2007/2013 O.O.2.1,  
22 B46D14002660009, “Il potenziamento e la riqualificazione del sistema delle infrastrutture nel settore  
23 dell’istruzione, della formazione e della ricerca”), for the FT-ICR mass spectrometer facilities, the  
24 Centro di Tecnologie Integrate per la Salute (CITIS, Project PONA3\_00138), Università di Salerno, for  
25 the 600 MHz NMR facilities.  
26  
27  
28  
29  
30  
31  
32  
33  
34  
35

36 **Supporting Information:** Copies of 1D, 2D NMR and HR MS spectra of new compounds, UV–vis  
37 absorption and fluorescence spectra of **2**, cyclic voltammetry of **2**, emission spectrum of **2** in  
38 dichloromethane at  $\lambda_{\text{exc}} = 390$  nm, emission spectrum of **2** in dichloromethane at  $\lambda_{\text{exc}} = 484$  nm,  
39 cartesian coordinates of the conformer I and III (Figure 4), this material is available free of charge via  
40 the Internet at <http://pubs.acs.org>.  
41  
42  
43  
44  
45  
46  
47  
48  
49

## 50 REFERENCES

51  
52 <sup>1</sup>(a) Jasti, R.; Bhattacharjee, J.; Neaton, J. B.; Bertozzi, C. R. *J. Am. Chem. Soc.* **2008**, *130*, 17646–  
53 17647. (b) Segawa, Y.; Miyamoto, S.; Omachi, H.; Matsuura, S.; Senel, P.; Sasamori, T.; Tokitoh, N.;  
54 Itami, K. *Angew. Chem., Int. Ed.* **2011**, *50*, 3244–3248. (c) Sisto, T. J.; Golder, M. R.; Hirst, E. S.; Jasti,  
55  
56  
57  
58  
59  
60

1 R. *J. Am. Chem. Soc.* **2011**, *133*, 15800–15802. (d) Xia, J.; Bacon, J. W.; Jasti, R. *Chem. Sci.* **2012**, *3*,  
2 3018–3021. (e) Darzi, E. R.; Jasti, R. *Chem. Soc. Rev.*, **2015**, *44*, 6401–6410. (f) Lewis, S. E. *Chem.*  
3 *Soc. Rev.*, **2015**, *44*, 2221–2304. (g) Zabula, A. V.; Filatov, A. S.; Xia, J.; Jasti, R.; Petrukhina, M. A.  
4 *Angew. Chem., Int. Ed.* **2013**, *52*, 5033–5036.

5  
6  
7  
8  
9  
10 <sup>2</sup>(a) Omachi, H.; Nakayama, T.; Takahashi, E.; Segawa, Y.; Itami, K. *Nat. Chem.* **2013**, *5*, 572–576.  
11  
12 (b) Segawa, Y.; Yagi, A.; Matsui, K.; Itami, K. *Angew. Chem. Int. Ed.* **2016**, *55*, 5136–5158. (c)  
13  
14 Golling, F. E.; Quernheim, M.; Wagner, M.; Nishiuchi, T.; Müllen, K. *Angew. Chem. Int. Ed.* **2014**, *53*,  
15 1525–1528. (d) Omachi, H.; Segawa, Y.; Itami, K. *Acc. Chem. Res.* **2012**, *45*, 1378–1389.

16  
17  
18  
19  
20 <sup>3</sup>(a) Iwamoto, T.; Watanabe, Y.; Sadahiro, T.; Haino, T.; Yamago, S. *Angew. Chem., Int. Ed.* **2011**, *50*,  
21 8342–8344. (b) Iwamoto, T.; Slanina, Z.; Mizorogi, N.; Guo, J.; Akasaka, T.; Nagase, S.; Takaya, H.;  
22  
23 Yasuda, N.; Kato, T.; Yamago, S. *Chem. Eur. J.* **2014**, *20*, 14403 – 14409. (c) Nakanishi, Y.; Omachi,  
24  
25 H.; Matsuura, S.; Miyata, Y.; Kitaura, R.; Segawa, Y.; Itami, K.; Shinohara, H. *Angew. Chem. Int. Ed.*  
26  
27 **2014**, *53*, 3102 –3106. (d) Ueno, H.; Nishihara, T.; Segawa, Y.; Itami, K. *Angew. Chem. Int. Ed.* **2015**,  
28  
29 *54*, 3707 –3711. (e) Lee, S.; Chénard, E.; Gray, D. L.; Moore, S. J. *J. Am. Chem. Soc.* **2016**, *138*,  
30  
31 13814–13817. (f) Very recently, Yamago and coworkers reported an example of inclusion of [n]CPPs  
32  
33 inside [n+5]CPPs macrocycles: Hashimoto, S.; Iwamoto, T.; Kurachi, D.; Kayahara, E.; Yamago, S.  
34  
35 *ChemPlusChem* **2017**, *82*, 1015–1020.

36  
37  
38  
39  
40  
41 <sup>4</sup> Della Sala, P.; Talotta, C.; Caruso, M.; De Rosa, M.; Soriente, A.; Neri, P.; Gaeta, C. *J. Org. Chem.*  
42  
43 **2017**, *82*, 9885–9889. C. Talotta, C. Gaeta, M. De Rosa, J. R. Ascenso, P. M. Marcos, P. Neri, *Eur. J.*  
44  
45 *Org. Chem.* **2016**, *1*, 158-167. De Rosa, M.; Talotta, C.; Soriente, A. *Lett. Org. Chem.* **2009**, *6*,  
46  
47 301–305.

48  
49  
50  
51 <sup>5</sup> Li, P.; Wong, B. M.; Zakharov, L. N.; Jasti, R. *Org. Lett.*, **2016**, *18*, 1574–1577.

<sup>6</sup>(a) Yagi, A.; Segawa, Y.; Itami, K. *J. Am. Chem. Soc.*, **2012**, *134*, 2962–2965. (b) Omachi, H.; Segawa, Y.; Itami, K. *Org. Lett.*, **2011**, *13*, 2480–2483. (c) Farajidizaji, B.; Huang, C.; Thakellapalli, H.; Li, S.; Akhmedov, N. G.; Popp, B. V.; Petersen, J. L.; Wang, K. K. *J. Org. Chem.* **2017**, *82*, 4458–4464.

<sup>7</sup>(a) Thakellapalli, H.; Farajidizaji, B.; Butcher, T. W.; Akhmedov, N. G.; Popp, B. V.; Petersen, J. L.; Wang, K. K. *Org. Lett.*, **2015**, *17*, 3470–3473. (b) Matsui, K.; Segawa, Y.; Itami, K. *Org. Lett.*, **2012**, *14*, 1888–1891. (c) Hayase, N.; Miyauchi, Y.; Aida, Y.; Sugiyama, H.; Uekusa, H.; Shibata, Y.; Tanaka, K. *Org. Lett.* **2017**, *19*, 2993–2996. (d) Nishigaki, S.; Fukui, M. Sugiyama, H.; Uekusa, H.; Kawauchi, S.; Shibata, Y.; Tanaka, K. *Chem. Eur. J.* **2017**, *23*, 7227–7231.

<sup>8</sup>(a) Balushev, S.; Miteva, T.; Yakutkin, V.; Nelles, G.; Yasuda, A.; Wegner, G. *PhysRevLett* **2006**, *97*, 143903-1-143903-3. (b) Singh-Rachford, T. N.; Castellano, F. N. *Coord. Chem. Rev.*, **2010**, *254*, 2560–2573.

<sup>9</sup>Monguzzi, A.; Braga, D.; Gandini, M.; Holmberg, V. C.; Kim, D. K.; Sahu, A.; Norris, D. J.; Meinardi, F. *Nano Lett.* **2014**, *14*, 6644–6650.

<sup>10</sup>(a) Khnayzer, R. S.; Blumhoff, J.; Harrington, J. A.; Haefele, A.; Deng, F.; Castellano, F. N. *Chem. Commun.* **2012**, *48*, 209–211. (b) Ye, C.; Wang, J.; Wang, X.; Ding, P.; Liang, Z.; Tao, X. *Phys. Chem. Chem. Phys.* **2016**, *18*, 3430–3437.

<sup>11</sup>Liu, Q.; Feng, W.; Yang, T.; Yi, T.; Li, F. *Nat. Protoc.* **2013**, *8*, 2033–2044.

<sup>12</sup>(a) Koslov, D. V.; Castellano, F. N. *Chem. Commun.* **2004**, 2860–2861. (b) Islangulov, R. R.; Lott, J.; Weder, C.; Castellano, F. N. *J. Am. Chem. Soc.* **2007**, *129*, 12652–12653. (c) Keivanidis, P. E.; Balushev, S.; Miteva, T.; Nelles, G.; Scherf, U.; Yasuda, A.; Wegner, G. *Adv. Mater.* **2003**, *15*, 2095–2098.

<sup>13</sup>Balushev, S.; Yakutkin, V.; Miteva, T.; Wegner, G.; Roberts, T.; Nelles, G.; Yasuda, A.; Chernov, S.; Aleshchenkov, S.; Cheprakov, A. *New J. Phys.* **2008**, *10*, 013007/1.

- 1  
2  
3  
4  
5  
6  
7  
8  
9  
10  
11  
12  
13  
14  
15  
16  
17  
18  
19  
20  
21  
22  
23  
24  
25  
26  
27  
28  
29  
30  
31  
32  
33  
34  
35  
36  
37  
38  
39  
40  
41  
42  
43  
44  
45  
46  
47  
48  
49  
50  
51  
52  
53  
54  
55  
56  
57  
58  
59  
60
- <sup>14</sup> Liu, Q.; Yang, T.; Feng, W.; Li, F. *J. Am. Chem. Soc.*, **2012**, *134*, 5390–5397.
- <sup>15</sup> Duan, P.; Yanai, N.; Nagatomi, H.; Kimizuka, N. *J. Am. Chem. Soc.*, **2015**, *137*, 1887–1894.
- <sup>16</sup> Adamska, L.; Nayyar, I.; Chen, H.; Swan, A. K.; Oldani, N.; Fernandez-Alberti, S.; Golder, M. R.; Jasti, R.; Doorn, S. K.; Tretiak, S. *Nano Lett.* **2014**, *14*, 6539–6546.
- <sup>17</sup> Iwamoto, T.; Watanabe, Y.; Sakamoto, Y.; Suzuki, T.; Yamago, S. *J. Am. Chem. Soc.*, **2011**, *133*, 8354–8361.
- <sup>18</sup> Fujitsuka, M.; Cho, D. W.; Iwamoto, T.; Yamago, S.; Majima, T. *Phys Chem. Chem. Phys.* **2012**, *14*, 14585–14588.
- <sup>19</sup> Segawa, Y.; Fukazawa, A.; Matsuura, S.; Omachi, H.; Yamaguchi, S.; Irle, S.; Itami, K. *Org. Biomol. Chem.*, **2012**, *10*, 5979–5984.
- <sup>20</sup> Golder, M. R.; Jasti, R. *Acc. Chem. Res.* **2015**, *48*, 557–566.
- <sup>21</sup> Du, H.; Fuh, R.-C. A.; Li, J.; Corkan, L. A.; Lindsey, J. S.; *Photochem. Photobiol.* **1998**, *68*, 141–142.
- <sup>22</sup> Williams, A. T. R.; Winfield, S. A.; Miller, J. N. *Analyst*, **1983**, *108*, 1067–1071.
- <sup>23</sup> (a) Parker, C. A.; Hatchard, C. G. *Proc. Chem Soc.*, London **1962**, 386–387. (b) Haefele, A.; Blumhoff, J.; Khnayzer, R. S.; Castellano, F. N. *J. Phys. Chem. Lett.* **2012**, *3*, 299–303. (c) Deng, F.; Blumhoff, J.; Castellano, F. N. *J. Phys. Chem. A* **2013**, *117*, 4412,4419.
- <sup>24</sup> Schwabe, T.; Grimme, S. *Phys. Chem. Chem. Phys.* **2006**, *8*, 4398–4401
- <sup>25</sup> Masson, E. *Org. Biomol. Chem.* **2013**, *11*, 2859–2871.
- <sup>26</sup> Yanai, T.; Tew, D. P.; Handy, N. C. *Chem. Phys. Lett.* **2004**, *393*, 51–57.

1 <sup>27</sup>Capobianco, A.; Borrelli, R.; Landi, A.; Velardo, A.; Peluso, A. *J Phys. Chem A*, **2016**, *120*, 5581-  
2 5589.  
3

4  
5 <sup>28</sup>Capobianco, A.; Velardo, A.; Peluso, A. *Comp. Theor. Chem.* **2015**, *1070*, 68-75; Capobianco, A.;  
6 Caruso, T.; Peluso, A. *Phys. Chem. Chem. Phys.* **2015**, *17*, 4750-4756.  
7

8  
9  
10 <sup>29</sup>Miertuš, S.; Scrocco, E.; Tomasi, J. *Chem. Phys.* **1981**, *55*, 117-129.  
11

12  
13  
14 <sup>30</sup>[G09]Frisch, M. J.; et al. *Gaussian 09*, Revision D.01; Gaussian Inc.: Wallingford, CT, 2009.  
15  
16  
17  
18  
19  
20  
21  
22  
23  
24  
25  
26  
27  
28  
29  
30  
31  
32  
33  
34  
35  
36  
37  
38  
39  
40  
41  
42  
43  
44  
45  
46  
47  
48  
49  
50  
51  
52  
53  
54  
55  
56  
57  
58  
59  
60